Supplementary Information

Multilayer meso-microporous carbon nanomesh: An effective oxygen reduction electrocatalyst

Fuping Zhang [a, c], Chenchen Ji [b] *, Chunmei Deng [b, c], Yinglin Zhang [a], Tingting Wei [b], Bo Xing [c], Liang Jiang [c], Yi Wang [c], Guo Yang [c], Yulin Shi [a, b, *]

[a] *School of Chemistry and Chemical Engineering, Key Laboratory for Green Processing of Chemical Engineering of Xinjiang Bingtuan, Shihezi University, Shihezi 832003, P.R. China.*

[b] *State Key Laboratory of Chemistry and Utilization of Carbon Based Energy Resources, School of Chemical Engineering and Technology, Xinjiang University, Urumqi 830017, P.R. China.*

[c] *College of Chemical Engineering, Sichuan University of Science and Engineering, Zigong 643000, P.R. China.*

* Corresponding author.

Email addresses: jichenchen2010@163.com (C. Ji), shiyulin521@126.com (Y. Shi).

Reagents and materials

In this work, we used 2-methylimidazole (2-MeIM, 98.0 wt.%, Adamas-beta), zinc acetate dihydrate ($Zn(OAc)\cdot 2H_2O$, 99.0 wt.%, General-reagent®), zinc chloride ($ZnCl_2$, 98.0 wt.%, Tianjin ShengAo Chemical Reagent Co., Ltd.), zinc sulfate heptahydrate ($ZnSO_4\cdot 7H_2O$, 99.5 wt.%, Tianjin Basf Chemical Co. Ltd), zinc nitrate hexahydrate ($Zn(NO_3)_2\cdot 6H_2O$, 99.0 wt.%, Tianjin Fuchen Chemicals Reagent Factory), and sodium chloride (NaCl, 99.5 wt.%, Tianjin ShengAo Chemical Reagent Co., Ltd.) as the reagents and materials.

Materials characterization

To characterize the materials we used SEM (ZEISS Sigma 300, Germany), TEM (HT7700, Japan), HRTEM (FEI Tecnai G2 F20, USA), AFM (Bruker Dimension Icon, Germany), XRD (Bruker D8 Advance, Germany), TG-DSC (TA SDT Q600 V20.9, USA), N_2 adsorption-desorption tests (Micrometrics ASAP 2460, USA), Raman (Thermo Fisher DXRxi, USA) with a 532 nm laser, XPS (Thermo Scientific ESCALAB 250Xi, USA), ICP-OES (Agilent 5110, USA) for measurements.

Electrochemical measurements

All the ORR activity was measured on a CHI 760E (Chenhua, China) electrochemical workstation with the three-electrode system. The catalyst ink was obtained by mixing 4.0 mg sample, 880 μL of ethanol, 100 μL of water and 20 μL of Nafion solution (5 wt%) and sonicating for 30 min. A certain amount of catalyst ink was pipetted on to glassy carbon rotating disk electrode (RDE, 3.0 mm diameter) or rotating ring disk electrode (RRDE, 5.61 mm diameter, a Pt ring:6.25 mm inner

diameter, 7.92 mm outer diameter) with a mass loading of 0.4 mg·cm^{-2}, where the electrode is the working electrode. For comparison, the mass loading of commercial Pt/C is also 0.4 mg·cm^{-2}. KCl-saturated Ag/AgCl electrode and Pt wire were used as the reference electrode and counter electrode, respectively. In this work, all the measured potentials were transformed to the reversible hydrogen electrode (RHE) potentials by using Eq. (1).

$$E(\text{vs. RHE}) = E(\text{vs.Ag/AgCl}) + 0.0591\text{pH} + 0. \quad (1)$$

The cyclic voltammetry (CV) polarization curves were recorded in O_2/N_2 saturated 0.1 M KOH solution at a scan rate of 50 mV s^{-1}. Linear sweep voltammetry (LSV) polarization curves were recorded at different rotation rates at 10 mV s^{-1}. The *i-t* curve was collected at a potential of 0.7 V (vs. RHE) and at a rotating rate of 400 rpm. The accelerated degradation test (ADT) was employed to assess the stability of catalyst: LSV curves were collected before and after 10, 000 cycles using CV from 0.6 V to 1.0 V at 100 mV s^{-1}. The methanol tolerance ability was tested by injecting methanol (10% *v*/*v*) in the 0.1 M KOH electrolyte during *i-t* measurement at 0.7 V.

The electron transfer number (*n*) was calculated from the LSV curves by using the Koutecký–Levich (K-L) equations [Eqs. (2), (3)].

$$\frac{1}{J} = \frac{1}{J_K} + \frac{1}{J_L} = \frac{1}{J_K} + \frac{1}{B\omega^{0.5}} \quad (2)$$

$$B = 0.62nF(D_{O_2})^{2/3}C_{O_2}v^{-1/6} \quad (3)$$

where J (mA cm^{-2}), J_L and J_K are the tested, diffusion-limiting and kinetic current densities, respectively. ω (rad s^{-1}) is the angular velocity of the RDE electrode, F is the

Faraday constant (96, 485 C mol^{-1}), D_{O_2} and C_{O_2} are the O_2 diffusion coefficient (1.9×10^{-5} cm^2 s^{-1}) and O_2 concentration in 0.1 M KOH, respectively., v is the kinematic viscosity of the electrolyte (0.01 cm^2 s^{-1}).

The peroxide percentage (%HO_2^-) and the n and were determined by RRDE operated at 1600 rpm in 0.1 M KOH, calculating by the following equations [Eqs. (4), (5)].

$$\%\,HO_2^- = 200 \times \frac{I_r/N}{I_r + I_r/N}\% \quad (4)$$

$$n = 4 \times \frac{I_d}{I_d + I_r/N} \quad (5)$$

where I_d and I_r are the stand disc current and ring current, respectively, and N represents the current collection efficiency of the Pt ring, N = 37%.

The double-layer capacitance (C_{dl}) is evaluated by the CV curves in the region from 1.1 to 1.2 V (vs. RHE) with the scan rates of 5, 10, 15, 20, 25, 30, 35, and 40 mV s^{-1}, which can be fitted by plotting the $(J_{anodic} - J_{cathodic})/2$ at 1.15 V (vs. RHE) against various scan rates, where J_{anodic} and $J_{cathodic}$ present anodic current density and cathodic current density, respectively.

The SEM, TEM, XRD and XPS measurements were carried out after stability test, where samples were uniformly distributed on carbon cloth (1 cm×1 cm) as work electrode and collected after ADT stability test.

Zn-air batteries assembly

To assemble Zn–air battery, a Zn plate with a thickness of 0.2 mm was used as anode, and 6.0 M KOH was employed as the electrolyte, and Celgard 2340 membrane

was used as a separator. For air cathode, the A-NC-M (2 mg), acetylene black (3 mg), and 60 wt.% poly tetra fluoroethylene (PTFE) emulsion (7 μL) were firstly dispersed into ethanol under sonication treatment and dry. Then, the mixture film (1*1 cm^2) was pressed onto the nickel foam substrate at 10 MPa. For comparison, Pt/C catalyst with loading of 0.2 mg_{Pt} cm^{-2} was also fabricated. All the electrochemical measurements of ZAB were conducted using the electrochemical workstation (CHI 760E, Shanghai).

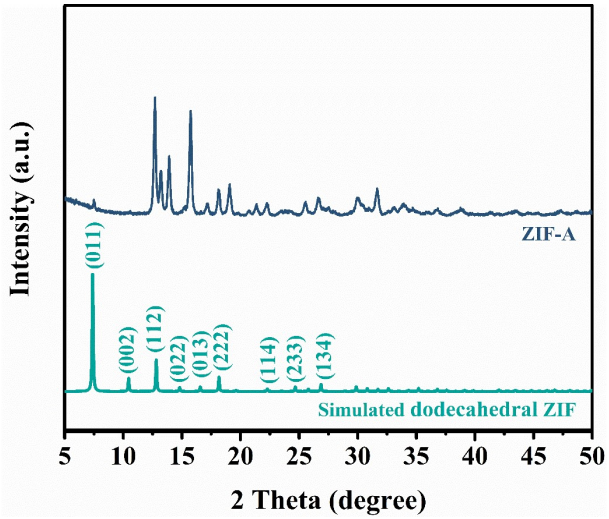

Figure S1. XRD plot of ZIF-A.

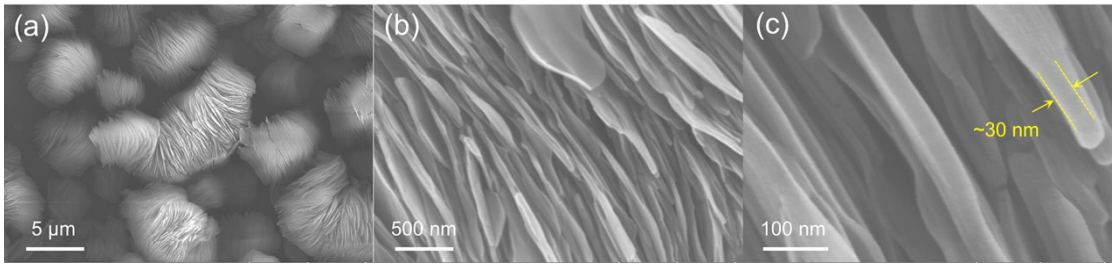

Figure S2. SEM images of ZIF-A at different magnifications.

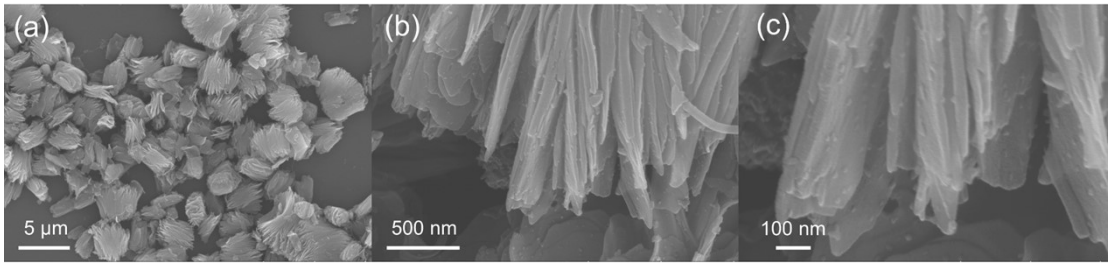

Figure S3. SEM images of A-NC-P at different magnifications.

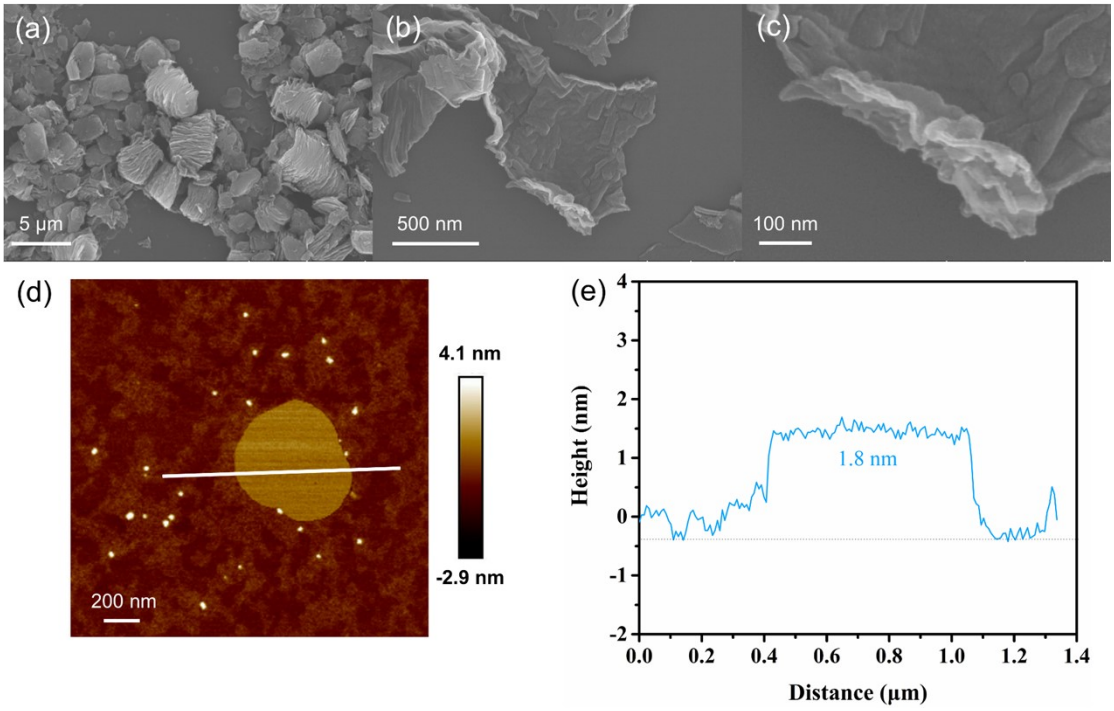

Figure S4. (a-c) SEM images of A-NC-M at different resolutions, (d) AFM image (e) and corresponding height profiles of the A-NC-M.

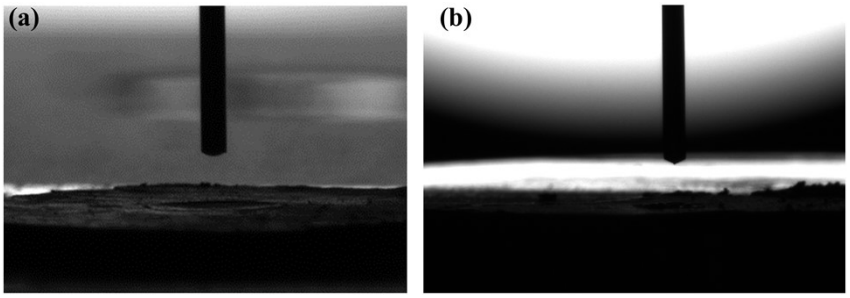

Figure S5. Water contact angle test of (a) A-NC-M and (b) A-NC-P.

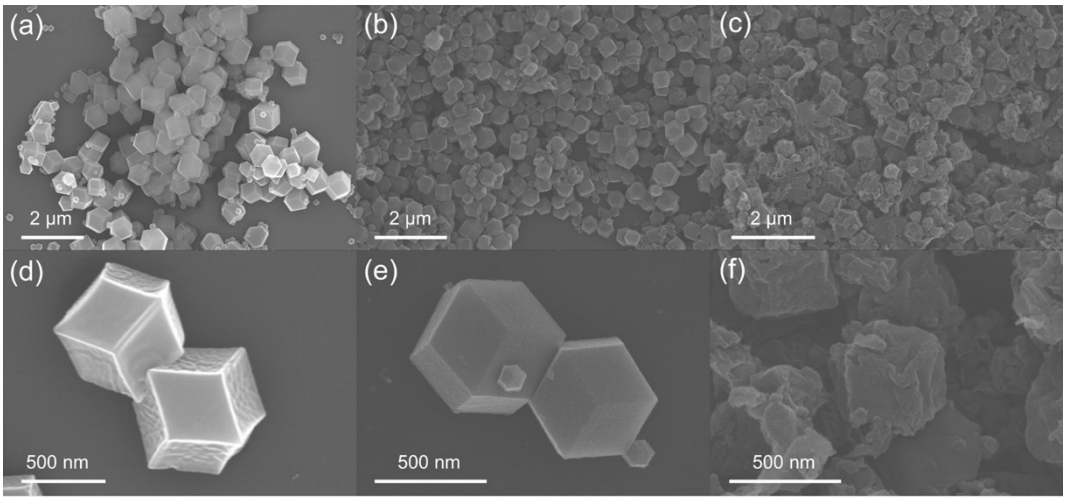

Figure S6. SEM images of (a, d) ZIF-P, (b, e) P-NC, and (c, f) P-NC/NaCl.

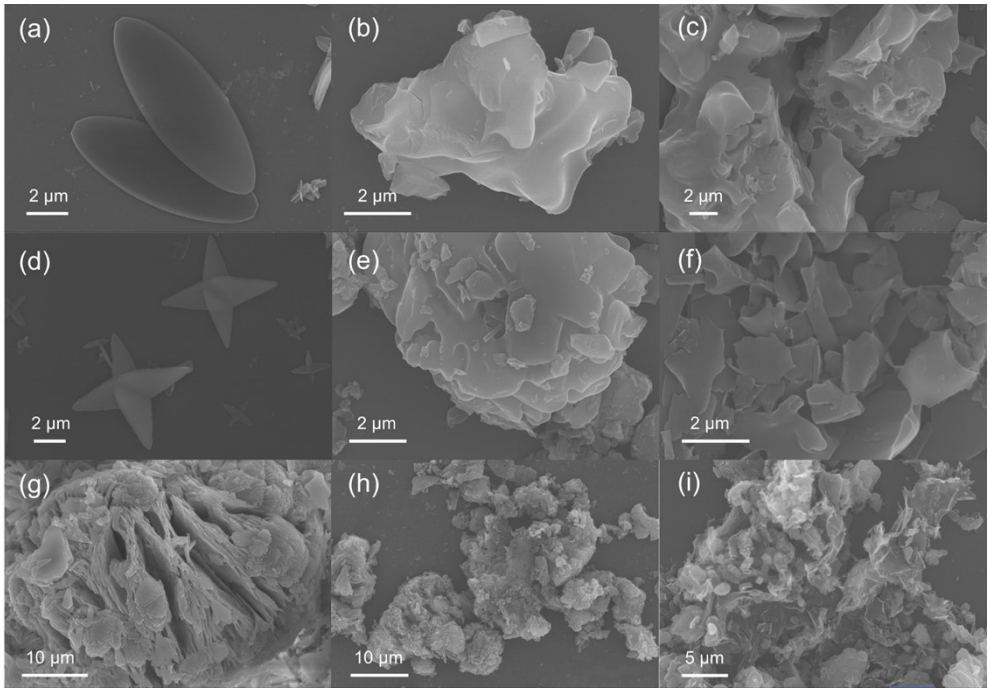

Figure S7. SEM images of (a) ZIF-NO_3^-, (b) NO_3^--NC, (c) NO_3^--NC/NaCl, (d) ZIF-Cl^-, (e) Cl^--NC, (f) Cl^--NC/NaCl, (g) ZIF-SO_4^{2-}, (h) SO_4^{2-}-NC, and (i) SO_4^{2-}-NC/NaCl

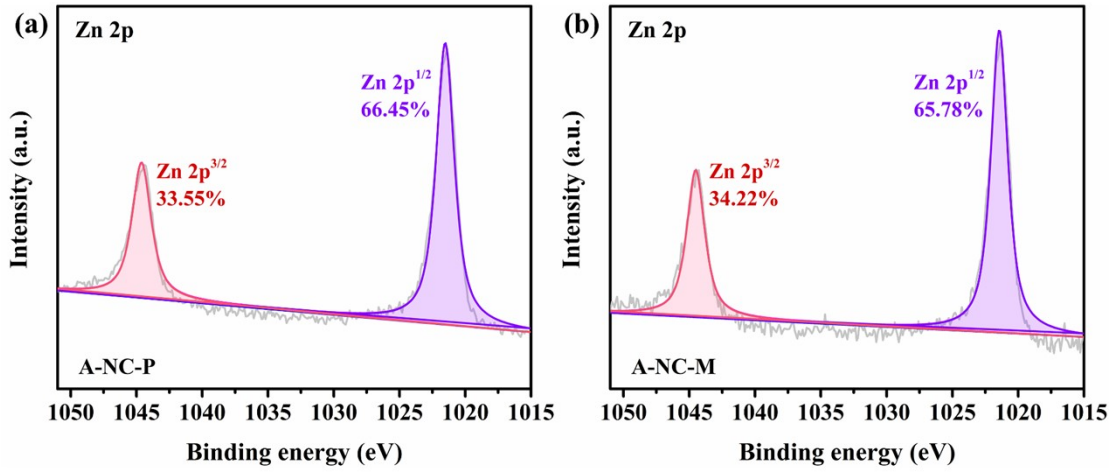

Figure S8. XPS N 1s spectra of (a) A-NC-P and (b) A-NC-M.

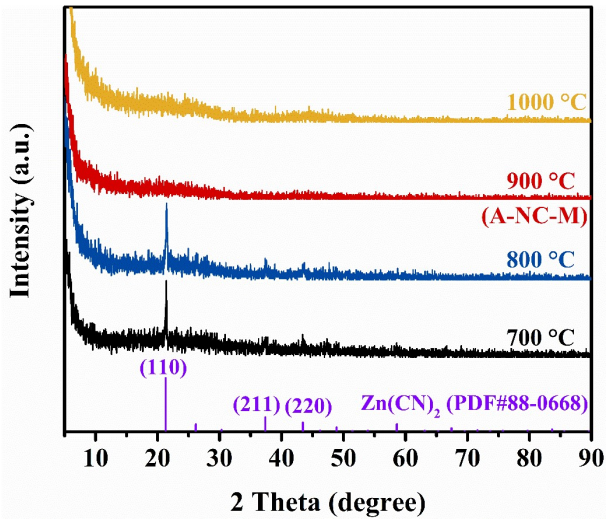

Figure S9. XRD plots of ZIF-A with NaCl pyrolyzed at different temperature (700~1000 °C).

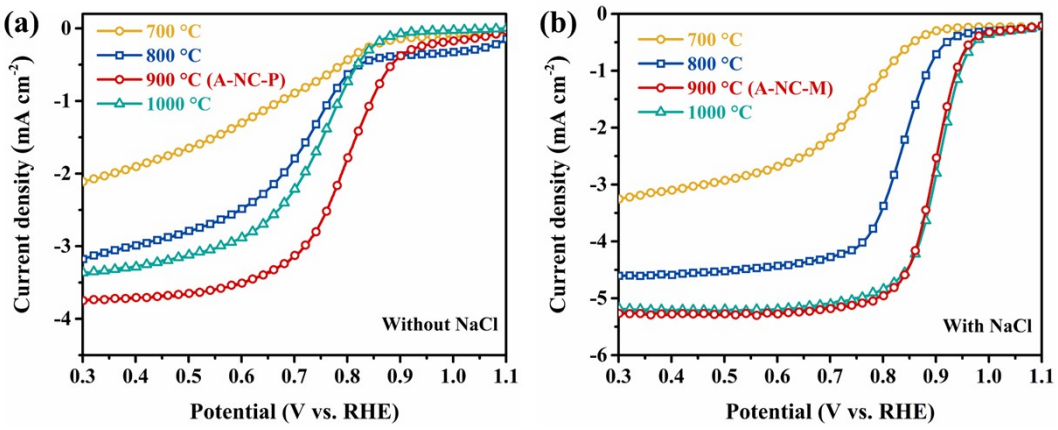

Figure S10. LSV curves of ZIF-A derived catalysts with different pyrolysis temperature (700, 800, 900 and 1000 °C): (a) without NaCl, (b) with NaCl.

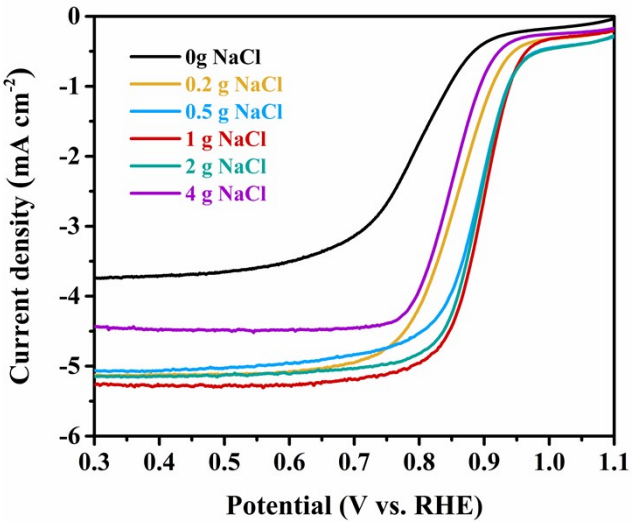

Figure S11. LSV curves of samples pyrolyzed with different amount of NaCl.

As is shown in **Figure S11**, in the absence of NaCl (i.e. A-NC-P), the catalyst shows the lowest $E_{1/2}$ value of 0.796 V. Upon the addition of a small quantity of NaCl (0.2 g), the $E_{1/2}$ increases to 0.859 V. Further increasing the NaCl amount to 1 g (i.e. A-NC-M) leads to the highest $E_{1/2}$ value of 0.899 V for the sample. However, when NaCl amount reaches 4 g, the $E_{1/2}$ decreases to 0.856 V. These results indicates that NaCl plays a critical role in the ORR performance of the resulting carbon materials. A low amount of NaCl would not enough to exfoliate and etch the ZIF-A derived carbon, while high NaCl ratio would excessively etch the carbon material, resulting in destroying the architecture of the resultant carbon.

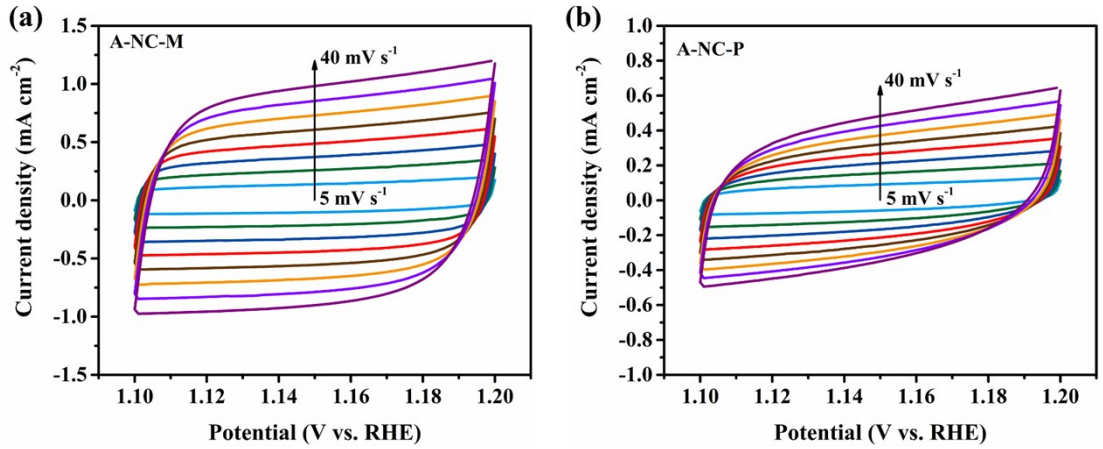

Figure S12. CV curves of (a) A-NC-M and (b) A-NC-P at the scan rates of 5, 10, 15, 20, 25, 30, 35, and 40 mV s^{-1}.

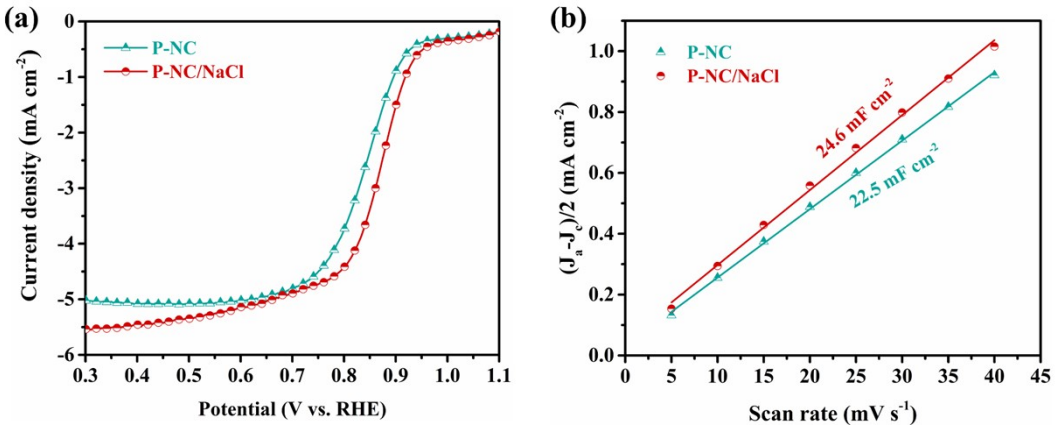

Figure S13. (a) LSV curves of P-NC and P-NC/NaCl at a scan rate of 10 mV s^{-1}; (b) Double-layer capacitance calculation of P-NC and P-NC/NaCl.

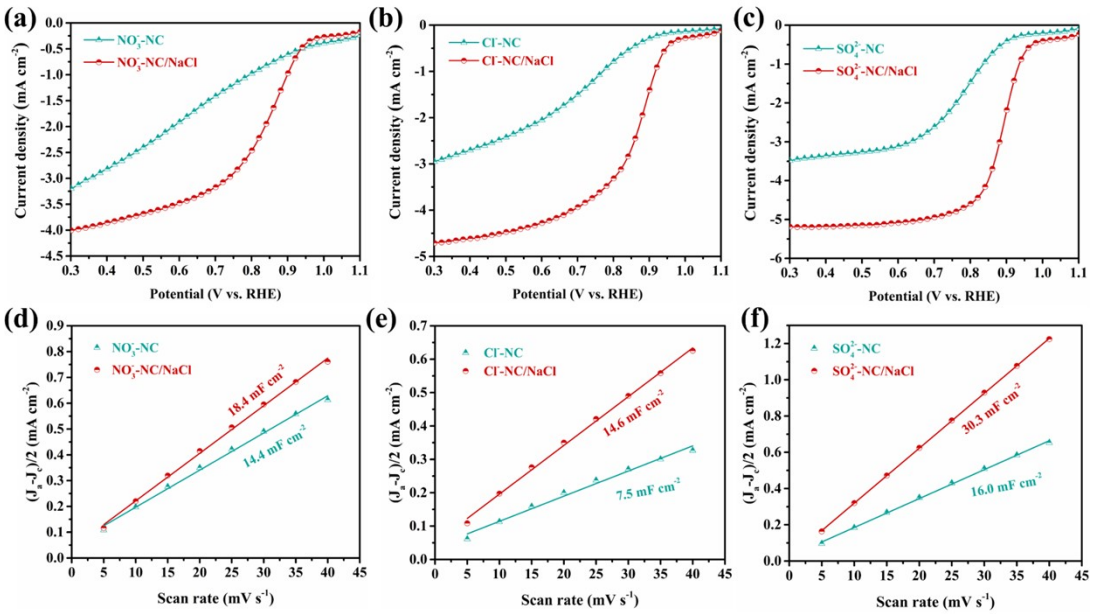

Figure S14. LSV curves of (a) NO_3^--NC, NO_3^--NC/NaCl; (b) Cl^--NC, Cl^--NC/NaCl and (c) SO_4^{2-}-NC, SO_4^{2-}-NC/NaCl at a scan rate of 10 mV s^{-1}. Double-layer capacitance calculation of (d) NO_3^--NC, NO_3^--NC/NaCl (e) Cl^--NC, Cl^--NC/NaCl, (f) SO_4^{2-}-NC, SO_4^{2-}-NC/NaCl.

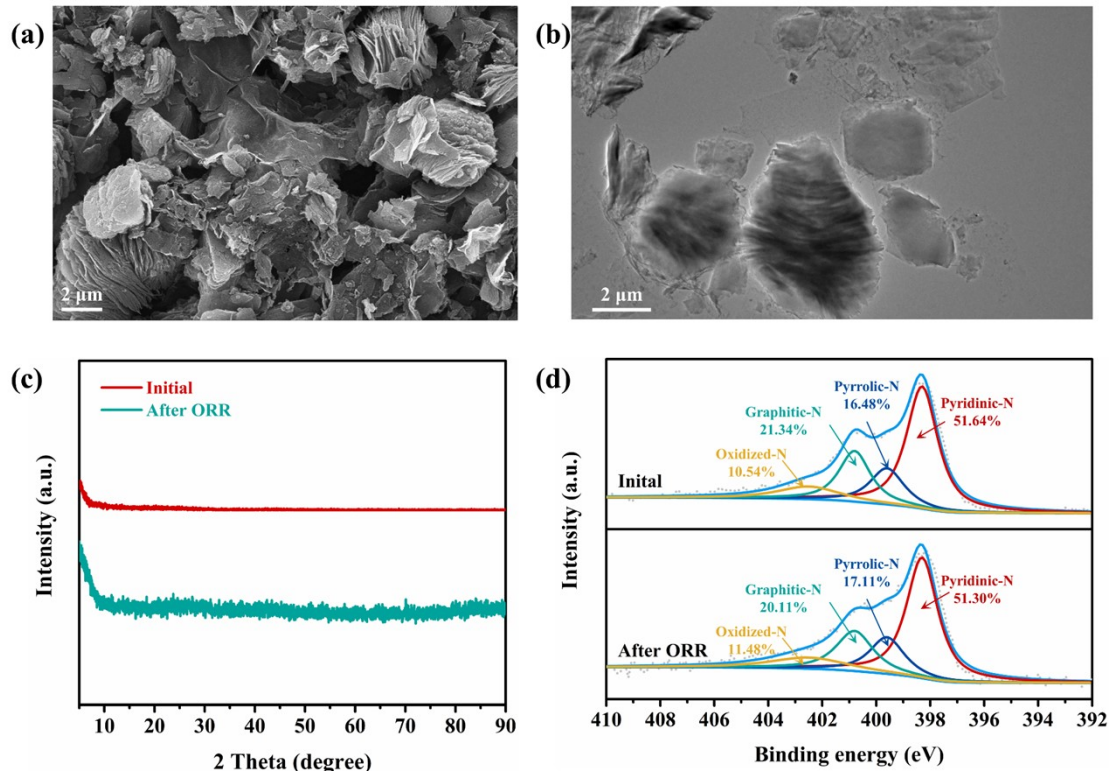

Figure S15. (a) SEM, (b) TEM images of A-NC-M after 10,000 cycles of ORR ADT; (c) XRD plots, (d) XPS N 1s spectra of A-NC-M before and after 10,000 cycles of ORR ADT.

Table S1 Surface atom contents of samples from XPS.

Sample	C 1s (at. %)	N 1s (at. %)	O 1s (at. %)	Zn 2p (at. %)
A-NC-P	80.83	9.94	7.62	1.61
700 °C	67.59	17.93	8.89	5.58
800 °C	72.62	13.49	9.3	4.59
900 °C (A-NC-M)	82.67	8.24	8.14	0.95
1000 °C	89.22	5.54	5.1	0.14

Table S2. The Zn content measured by ICP-OES measurements.

Sample	Zn (wt.%)
A-NC-P	11.08
A-NC-M	3.77

Table S3 Comparison of the ORR properties between A-NC-M and some catalysts reported in the literature

Catalysts	Electrolyte	$E_{1/2}$ / V	References
V-Co_9S_8	0.1 M KOH	0.83	1
MNCSs	0.1 M KOH	0.82	2
Fe/SNCFs-NH_3	0.1 M KOH	0.89	3
O–Co–N/C	0.1 M KOH	0.85	4
Co SAs@PNCN	0.1 M KOH	0.851	5
Fe-N/HPC-1000	0.1 M KOH	0.881	6
Co_2N/CoP@PNCNTs	0.1 M KOH	0.85	7
CoFe-SNC	0.1 M KOH	0.86	8
MS-CoSA-N-C-800°C	0.1 M KOH	0.86	9
0.05CoO_x@PNC	0.1 M KOH	0.88	10
CoFeN-NCNTs//CCM	0.1 M KOH	0.84	11
3DOM Fe/Co@NC-WO_{2-x}	0.1 M KOH	0.87	12
Co@N, S–C	0.1 M KOH	0.894	13
FeNi-SAs@NC	0.1 M KOH	0.907	14
Ni@N-HCGHF	0.1 M KOH	0.875	15
A-NC-M	0.1 M KOH	0.899	This work

References

1. L. Wu, S. Li, L. Li, H. Zhang, L. Tao, X. Geng, H. Yang, W. Zhou, C. Sun, D. Ju and B. An, *Appl. Catal. B: Environ.* , 2023, **324**, 122250.
2. Z. Zhao, L. Duan, Y. Zhao, L. Wang, J. Zhang, F. Bu, Z. Sun, T. Zhang, M. Liu, H. Chen, Y. Yang, K. Lan, Z. Lv, L. Zu, P. Zhang, R. Che, Y. Tang, D. Chao, W. Li and D. Zhao, *J. Am. Chem. Soc.*, 2022, **144**, 11767-11777.
3. L. Yang, X. Zhang, L. Yu, J. Hou, Z. Zhou and R. Lv, *Adv. Mater.*, 2021, **34**, 2105410.
4. W. Zhang, C. H. Xu, H. Zheng, R. Li and K. Zhou, *Adv. Funct. Mater.*, 2022, **32**, 2200763.
5. M. Zhang, H. Li, J. Chen, F. X. Ma, L. Zhen, Z. Wen and C. Y. Xu, *Small*, 2022, **18**, 2202476.
6. H. Zhang, W. Xia, J. Ge and J. Tang, *Chem. Eng. J.*, 2022, **429**, 132214.
7. C. Yao, J. Li, Z. Zhang, C. Gou, Z. Zhang, G. Pan and J. Zhang, *Small*, 2022, **18**, 2108094.
8. C.-C. Weng, J.-T. Ren, H.-Y. Wang, X.-W. Lv, Y.-J. Song, Y.-S. Wang, L. Chen, W.-W. Tian and Z.-Y. Yuan, *Appl. Catal. B: Environ.* , 2022, **307**, 121190.
9. K. Wang, Z. Lu, J. Lei, Z. Liu, Y. Li and Y. Cao, *ACS Nano*, 2022, **16**, 11944-11956.
10. Y. Tan, W. Zhu, Z. Zhang, W. Wu, R. Chen, S. Mu, H. Lv and N. Cheng, *Nano Energy*, 2021, **83**, 105813.
11. G. Zhou, G. Liu, X. Liu, Q. Yu, H. Mao, Z. Xiao and L. Wang, *Adv. Funct. Mater.*,

2021, **32**, 2107608.

12. Q. Han, X. Zhao, Y. Luo, L. Wu, S. Sun, J. Li, Y. Wang, G. Liu and Z. Chen, *Adv. Sci.*, 2022, **9**, e2104237.

13. D. Lyu, S. Yao, A. Ali, Z. Q. Tian, P. Tsiakaras and P. K. Shen, *Adv Energy Mater*, 2021, **11**, 2101249.

14. F. Luo, J. Zhu, S. Ma, M. Li, R. Xu, Q. Zhang, Z. Yang, K. Qu, W. Cai and Z. Chen, *Energy Stor. Mater.*, 2021, **35**, 723-730.

15. L. Yan, Y. Xu, P. Chen, S. Zhang, H. Jiang, L. Yang, Y. Wang, L. Zhang, J. Shen, X. Zhao and L. Wang, *Adv. Mater.*, 2020, **32**, 2003313.